DYNAMIC DEFORMATION OF A SOLENOID WIRE
DUE TO INTERNAL MAGNETIC PRESSURE

E. L. Ruden[*], G. F. Kiuttu

Air Force Research Laboratory, Directed Energy Directorate, 3550 Aberdeen Ave SE
Kirtland AFB, New Mexico, USA

M. H. Frese, S. D. Frese
Numerex, 2309 Renard Place SE
Albuquerque, NM, USA

Abstract

Deformation of the wire used in the solenoidal windings of an inertially confined pulsed high magnetic field generator is potentially the limiting factor for the magnitude and duration of the magnetic field produced. The rising magnetic pressure at the wire surface can become large enough to cause the cross section of the wire to deform on a time scale shorter than overall solenoid disassembly time. This may result in short circuiting due to insulator breakage and/or physical contact of adjacent windings. An analytic approximation modeling the deformation dynamics is presented which takes into account both inertial and material yield strength effects. The model is validated by comparison to two dimensional magnetohydrodynamic simulations of the process by Numerex's MS Windows version of AFRL's MACH2. Cases where yield strength has a negligible effect on the deformation, and where yield strength is significant are considered.

I. INTRODUCTION

Consider a long solenoid wound from round wire made of metal with a given yield strength and having a diameter small compared to the solenoid diameter. We wish to analytically model the deformation magnitude of the wire due to an internal magnetic pressure high enough to cause rapid disassembly. We represent the wire in planar geometry by a square one of the same area that, by assumption, remains rectangular during deformation to make the problem more tractable. The solenoid radius is assumed to be large enough to permit hoop stress effects to be neglected during the time of interest. The magnetic pressure is represented by a uniform pressure applied to one side of the wire that rises instantaneously to a constant value P at time $t = 0$. A free standing wire and one bounded by a rigid wall on the side opposite the pressurized side are considered. These are intended to represent a free standing solenoid and one reinforced by a surrounding tube, respectively. The dynamic width of the wire is calculated assuming conservation of global energy and momentum.

The relationship between P used in the model and the central solenoid magnetic field B_1 must take into account the fact that the local magnetic field at the wire surface is higher than B_1. To determine an effective P, we equate the initial pdV work performed per winding of an ideal solenoid by expanding its radius by dR. to the work performed by pressure P to our square wire over the same displacement,

$$\frac{B_1^2}{2\mu_0} \times 2\pi R_0 S dR = P \times 2\pi R_0 A_0 dR \qquad (1)$$

Here, R_0 is the initial solenoid radius, S is the wire spacing, r_0 is the initial wire radius, A_0 is the initial side length of a square wire of the same area, and $\mu_0 = 4\pi \times 10^{-7}$ H m^{-1}. From this,

$$P = \frac{S}{A_0} \frac{B_1^2}{2\mu_0} \qquad \text{where} \qquad A_0 = \sqrt{\pi} r_0 \qquad (2)$$

The models are checked against the code MACH2[1][2] for a range of conditions to establish their suitability for providing general design criteria for similar geometries.

II. DEFORMATION OF A FREE RECTANGULAR WIRE DUE TO PRESSURE ON ONE SIDE

Referring to "top" and "bottom" as illustrated in Fig. 1, we first calculate the deformation of a free rectangular wire (for generality) due a uniform and constant pressure P on the top surface, assuming the wire remains rectangular. We define our (x,y) coordinates to be in the accelerating reference frame of the wire, with the origin at the center of mass. The dynamic wire width is A (A_0 initially), the height is B (B_0 initially), and the center of mass speed is V. Uniaxial yield strength Y and density ρ are assumed constant. We further assume the simplest possible expression for the material velocity field in the

Report Documentation Page

1. REPORT DATE **JUN 2001**	2. REPORT TYPE **N/A**	3. DATES COVERED **-**

4. TITLE AND SUBTITLE	5a. CONTRACT NUMBER
Dynamic Deformation Of A Solenoid Wire Due To Internal Magnetic Pressure	5b. GRANT NUMBER
	5c. PROGRAM ELEMENT NUMBER
6. AUTHOR(S)	5d. PROJECT NUMBER
	5e. TASK NUMBER
	5f. WORK UNIT NUMBER

7. PERFORMING ORGANIZATION NAME(S) AND ADDRESS(ES) **Air Force Research Laboratory, Directed Energy Directorate, 3550 Aberdeen Ave SE Kirtland AFB, New Mexico, USA**	8. PERFORMING ORGANIZATION REPORT NUMBER
9. SPONSORING/MONITORING AGENCY NAME(S) AND ADDRESS(ES)	10. SPONSOR/MONITOR'S ACRONYM(S)
	11. SPONSOR/MONITOR'S REPORT NUMBER(S)

12. DISTRIBUTION/AVAILABILITY STATEMENT
Approved for public release, distribution unlimited

13. SUPPLEMENTARY NOTES
See also ADM002371. 2013 IEEE Pulsed Power Conference, Digest of Technical Papers 1976-2013, and Abstracts of the 2013 IEEE International Conference on Plasma Science. IEEE International Pulsed Power Conference (19th). Held in San Francisco, CA on 16-21 June 2013. U.S. Government or Federal Purpose Rights License.

14. ABSTRACT
Deformation of the wire used in the solenoidal windings of an inertially confined pulsed high magnetic field generator is potentially the limiting factor for the magnitude and duration of the magnetic field produced. The rising magnetic pressure at the wire surface can become large enough to cause the cross section of the wire to deform on a time scale shorter than overall solenoid disassembly time. This may result in short circuiting due to insulator breakage and/or physical contact of adjacent windings. An analytic approximation modeling the deformation dynamics is presented which takes into account both inertial and material yield strength effects. The model is validated by comparison to two dimensional magnetohydrodynamic simulations of the process by Numerex's MS Windows version of AFRL's MACH2. Cases where yield strength has a negligible effect on the deformation, and where yield strength is significant are considered.

15. SUBJECT TERMS

16. SECURITY CLASSIFICATION OF:			17. LIMITATION OF ABSTRACT	18. NUMBER OF PAGES	19a. NAME OF RESPONSIBLE PERSON
a. REPORT **unclassified**	b. ABSTRACT **unclassified**	c. THIS PAGE **unclassified**	**SAR**	**4**	

center of mass frame **v** consistent with our rectangular cross section assumption,

$$v_x = \frac{dA}{dt}\frac{x}{A} \qquad v_y = \frac{dB}{dt}\frac{y}{B} \qquad v_z = 0 \qquad (3)$$

From incompressibility,
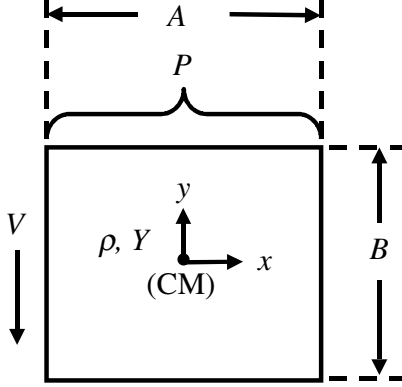
$$AB = A_0 B_0 \qquad (4)$$

Figure 1. Geometry for analytic model of free standing solenoid wire deformation.

The Levy-Mises equation for rigid plastic flow[3] is assumed,

$$\mathbf{S} = \sqrt{\frac{2}{3}}Y\mathbf{D}/\sqrt{\mathbf{D}\cdot\mathbf{D}}, \qquad (5)$$

where **S** is the deviatoric stress tensor (**S·I = 0**), and **D** is the deviatoric strain rate tensor,

$$\mathbf{D} = \frac{1}{2}\left(\nabla\mathbf{v} + \nabla\mathbf{v}^{\mathbf{T}}\right) - \frac{1}{3}\left(\nabla\cdot\mathbf{v}\right)\mathbf{I} \qquad (6)$$

Incompressibility implies,

$$\nabla\cdot\mathbf{v} = \mathbf{0} \qquad (7)$$

With this, substituting Eq. (3) into Eq. (6) gives,

$$D_{xx} = -\frac{1}{A}\frac{dA}{dt} \qquad D_{yy} = \frac{1}{B}\frac{dB}{dt} \qquad (8)$$

for the nonzero **D** terms.

The time derivatives of the external work, plastic work[3], and kinetic energy per unit length of wire are, respectively,

$$\frac{dW}{dt} = PA\left(V - \frac{1}{2}\frac{dB}{dt}\right) \qquad (9)$$

$$\frac{dE_p}{dt} = \int_{\text{Area}} (\mathbf{S}\cdot\mathbf{D})\,da \qquad (10)$$

$$\frac{dK}{dt} = \frac{d}{dt}\left(\frac{1}{2}\rho A_0 B_0 V^2 + \int_{\text{Area}}\frac{1}{2}\rho v^2 da\right) \qquad (11)$$

where the integrals are over the wire cross section. Conservation of energy implies,

$$\frac{dW}{dt} = \frac{dE_p}{dt} + \frac{dK}{dt} \qquad (12)$$

Substituting the **v**, **D**, **S** components from Eq. (3), Eq. (6), and Eq. (5), respectively, into the energy terms, and performing the integrations, this expression becomes,

$$PAV - \frac{1}{2}PA\frac{dB}{dt} = \sqrt{\frac{2}{3}}YAB\sqrt{\left(\frac{1}{A}\frac{dA}{dt}\right)^2 + \left(\frac{1}{B}\frac{dB}{dt}\right)^2}$$
$$+\rho A_0 B_0 V\frac{dV}{dt} + \frac{\rho}{24}\frac{d}{dt}\left[AB\left(\frac{dA}{dt}\right)^2 + AB\left(\frac{dB}{dt}\right)^2\right] \qquad (13)$$

Conservation of momentum implies,

$$PA = \rho A_0 B_0\frac{dV}{dt} \qquad (14)$$

This allows us to eliminate the terms with V in Eq. (13). B may be eliminated via Eq. (4), and the result integrated by time to obtain,

$$\frac{d\varepsilon}{dt} = \sqrt{\frac{24\left(P/2 - 2Y/\sqrt{3}\right)\varepsilon}{\rho\left(B_0^2 e^{-2\varepsilon} + A_0^2 e^{2\varepsilon}\right)}} \quad \text{where } \varepsilon = \ln\frac{A}{A_0} \quad (15)$$

ε can be recognized as plastic strain. Solving for time gives,

$$t = \sqrt{\frac{\rho\left(B_0^2 + A_0^2\right)}{24\left(P/2 - 2Y/\sqrt{3}\right)}}\int_0^\varepsilon\sqrt{\frac{B_0^2 e^{-2s} + A_0^2 e^{2s}}{s\left(B_0^2 + A_0^2\right)}}\,ds \qquad (16)$$

The integrand may be approximated by the truncated Laurent expansion in $s^{\frac{1}{2}}$,

$$s^{-\frac{1}{2}} - \alpha s^{\frac{1}{2}} + \left(1 - \frac{\alpha^2}{2}\right)s^{\frac{3}{2}} + \left(\frac{\alpha}{3} - \frac{\alpha^3}{2}\right)s^{\frac{5}{2}} \qquad (17)$$

This permits integration giving the following approximation accurate for small strains ($\varepsilon \sim 0.1$),

$$t \approx \sqrt{\frac{\rho \left(B_0^2 + A_0^2\right)}{3P - 4\sqrt{3}Y}} \left[\varepsilon^{\frac{1}{2}} - \frac{1}{3}\alpha\varepsilon^{\frac{3}{2}} + \frac{1}{5}\left(1 - \frac{\alpha^2}{2}\right)\varepsilon^{\frac{5}{2}} \right.$$

$$\left. + \frac{1}{7}\left(\frac{\alpha}{3} - \frac{\alpha^3}{2}\right)\varepsilon^{\frac{7}{2}} \right] \quad \text{where} \quad \alpha = \frac{B_0^2 - A_0^2}{B_0^2 + A_0^2} \quad (18)$$

We see from the denominator of the root that no flow occurs if $Y \geq 3^{\frac{1}{2}}P/4$.

$A_0 = B_0$ for an initially square wire, and Eq. (16) may be written,

$$t = \sqrt{\frac{2\rho A_0^2}{3P - 4\sqrt{3}Y}} \int_0^\varepsilon \sqrt{\cosh\left(2s^2\right)}\,ds \quad (19)$$

And, with $\alpha = 0$, Eq. (18) becomes,

$$t \approx \sqrt{\frac{2\rho A_0^2}{3P - 4\sqrt{3}Y}} \left(\varepsilon^{\frac{1}{2}} + \frac{1}{5}\varepsilon^{\frac{5}{2}}\right) \text{ for } A_0 = B_0 \quad (20)$$

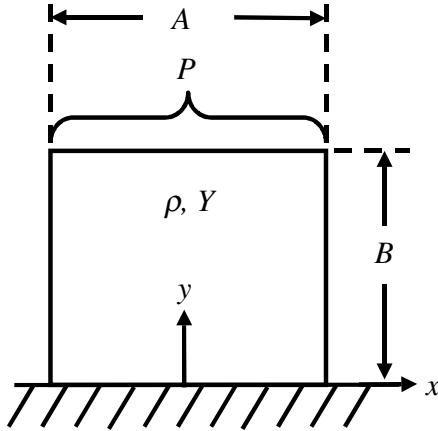## III. DEFORMATION OF A BOUNDED RECTANGULAR WIRE DUE TO PRESSURE ON ONE SIDE

Figure 2. Geometry for analytic model of externally bounded solenoid wire deformation.

A similar analysis is performed, but for a wire bounded from below as shown in Fig. 2. Qualitative differences in the calculation are that energy terms are evaluated in the stationary frame and conservation of momentum is not needed to simplify the energy balance equation. The corresponding time to reach strain ε in this case is,

$$t = \sqrt{\frac{\rho \left(4B_0^2 + A_0^2\right)}{24P - 16\sqrt{3}Y}} \int_0^\varepsilon \sqrt{\frac{4B_0^2 e^{-2s} + A_0^2 e^{2s}}{s\left(4B_0^2 + A_0^2\right)}}\,ds \quad (21)$$

which is approximated for $\varepsilon \sim 0.1$ by,

$$t \approx \sqrt{\frac{\rho \left(4B_0^2 + A_0^2\right)}{6P - 4\sqrt{3}Y}} \left[\varepsilon^{\frac{1}{2}} - \frac{1}{3}\beta\varepsilon^{\frac{3}{2}} + \frac{1}{5}\left(1 - \frac{\beta^2}{2}\right)\varepsilon^{\frac{5}{2}} \right.$$

$$\left. + \frac{1}{7}\left(\frac{\beta}{3} - \frac{\beta^3}{2}\right)\varepsilon^{\frac{7}{2}} \right] \quad \text{where} \quad \beta = \frac{4B_0^2 - A_0^2}{4B_0^2 + A_0^2} \quad (22)$$

We see from the denominator of the root that the yield strength must be twice as high in the supported case ($Y \geq 3^{\frac{1}{2}}P/2$) vs. the unsupported one to avoid flow. $\beta = 3/5$ for an initially square wire.
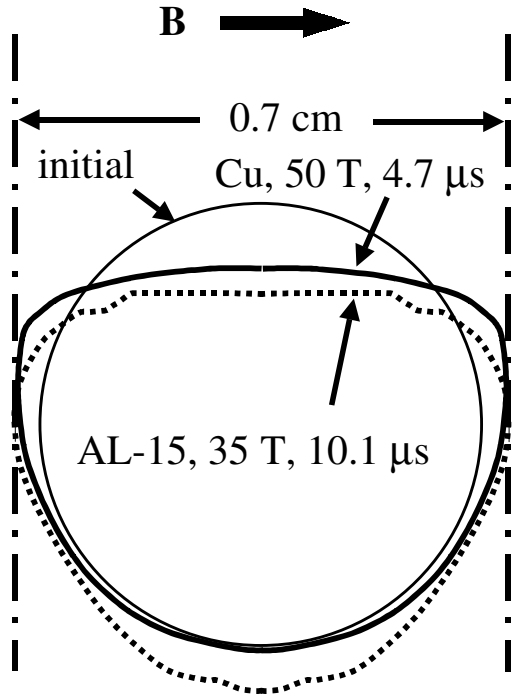
IV. COMPARISON WITH MACH2 SIMULATIONS

Figure 3. MACH2 results at 10% spread for two cases of solenoid wire deformation.

MACH2 simulations run in planar geometry representing a solenoid wound from wire of radius $r_0 = 3.18 \times 10^{-3}$ m and having a gap between turns equal to 10% of the wire diameter are compared to our analytic free and bounded wire models. We consider four cases with $B_1 = 35$ T and $B_1 = 50$ T using half-hard Cu and 90% cold worked Glidcop™ Al$_2$O$_3$ dispersion strengthened Cu alloy AL-15[4][5]. The latter has a density, compressive equation of state, conductivity, and elastic modulus similar to Cu, but a higher yield strength. The SESAME Cu equation of state table[6] and Desjarlais' modified[7] Lee-More Cu electrical conductivity model[8] are used for both materials. The Steinberg-Cochran-Guinan strain rate

independent half-hard Cu model[9] is used for Cu's elastic-plastic behavior. The same S-C-G shear modulus is used for AL-15 but, lacking high strain rate data, AL-15's uniaxial yield strength is set to its published value of 3.40×10^8 Pa. Periodic boundary conditions are invoked, corresponding to the wire being one of an infinite array of wires with center-to-center spacing of 7×10^{-3} m. The upper boundary condition at $y = 0.10$ m is defined to have a magnetic field of $\mathbf{B} = B_1\mathbf{x}$, keeping the same "up-down" convention as the analytic model. The lower boundary condition is at $y = -0.10$ cm with $\mathbf{B} = \mathbf{0}$. The simulations available to date are for free wires only. Fig. 3 illustrates the wire outlines for two cases at the time the wires expand by 10% and, therefore, short to the neighboring turns.

We compare the time t required for the wire to spread by 10% in the different models. With the help of Eq. (2) and Eq. (15), parameters for the analytic models common to all cases considered are,

$$S = 7.00 \times 10^{-3} \text{ m} \qquad \rho = 8930 \text{ kg m}^{-3}$$
$$B_0 = A_0 = 5.64 \times 10^{-3} \text{ m} \quad \varepsilon = 0.0953$$
$$(23)$$

The equivalent pressures for $B_1 = 35$ T and $B_1 = 50$ T are, from Eq. (15), $P = 6.05 \times 10^8$ Pa and $P = 1.24 \times 10^9$ Pa, respectively. Using the high strain rate initial yield strength from half-hard Cu's S-C-G model and the published yield strength of AL-15, we use $Y = 1.23 \times 10^8$ Pa and $Y = 3.4 \times 10^8$ Pa, respectively, for the analytic models. Table 1 summarizes the spread times determined by Eq. (20), Eq. (22), and MACH2.

Table 1. Times for wire to spread 10%

Case	Free	Bound	MACH
Cu, 35 T	7.50	6.85	7.0
Al-15, 35 T	Stable	10.11	10.1
Cu, 50 T	4.36	4.46	4.7
AL-15, 50 T	6.34	5.08	5.7

Y plays only a small role in the dynamics and the three models are in reasonable agreement in all cases but the second. One may infer from the small displacement of the bottom of the wire for Cu at 50 T illustrated in Fig. 3 that a bounding wall does not have enough time to affect the wire width by the time the wire spreads 10% in the inertially confined limit. Both analytic models reflect this accurately.

It comes as a surprise in the second case, however, that MACH2 agrees much better with the analytic bounded wire model than with the free wire model that was intended to represent it. In fact, the latter model predicts that the wire does not deform at all in this case ($Y \geq 3^{\frac{1}{2}}P/4$). It appears that in cases such as this where Y *does* play a significant role in impeding expansion, Eq. (22) provides the best guidance. Though not yet fully understood, Fig. 3 suggests an explanation. The wire's shape at 10% expansion varies little with the relative

values of Y and B_1. Furthermore, the deformation occurs primarily in the top half before the bottom is substantially displaced, at least for the cases explored here. Placing a lower boundary on the analytic model apparently offsets the error introduced by its unrealistically homogeneous deformation. It is not clear, however, that this would continue to be the case for significantly greater deformations, or if P were much closer to the critical value for flow in the bounded model (3.93×10^8 Pa for AL-15). These cases will be addressed in future calculations to better characterize the range of validity of Eq. (22).

V. REFERENCES

[1] M. H. Frese, "MACH2: A two-dimensional magneto-hydrodynamic simulation code for complex experimental configurations", Mission Research Corp., Albuquerque, NM, Tech. Rep. AMRC-R-874, 1987.
[2] R. E. Peterkin, Jr. and M. H. Frese, "A material strength capability for MACH2", Mission Research Corp, Albuquerque, NM, Tech. Rep. MRC/ABQ-R-1191, Nov., 1989.
[3] A. S. Kahn and S. Huang, Continuum Theory of Plasticity. NY: John Wiley & Sons, 1995.
[4] T. J. Miller, S. J. Zinkle, and B. A. Chin, "Strength and fatigue of dispersion strengthened copper", J. Nuclear Mater., 179-181, pp. 263-266, 1991.
[5] T. S. Srivatsan, N. Narendra, and J. D. Troxell, "Tensile deformation and fracture behavior of an oxide dispersion strengthened copper alloy", Materials and Design}, vol. 21, pp. 191-198, 2000.
[6] S. P. Lyon and J. D. Johnson (eds.), "SESAME: the Los Alamos National Laboratory equation of state database", LANL, Los Alamos, NM, Tech. Rep. LA-UR-92-3407, 1992.
[7] S. E. Rosenthal, M. P. Desjarlais, R. B. Spielman, W. A. Stygar, J. R. Asay, M. R. Douglas, M. H. Frese, R. L. Morse, and D. B. Reisman, "MHD modeling of conductors at ultrahigh current density", IEEE trans. Plasma Sci., vol.28, pp. 1427-1433, 2000.
[8] Y. T. Lee and R. M. More, "An electron conductivity model for dense plasma", Phys. Fluids, vol. 27, pp. 1273-1286, 1984.
[9] D. J. Steinberg, S. G. Cochran, and M. W. Guinan, "A constitutive model for metals applicable at high-strain rate", J. Appl. Phys., vol 51, pp. 1498-1504, 1980.
[10] D. J. Steinberg, "Equation of state and strength properties of selected materials (revised)" LLNL, Livermore, CA, Tech. Rep. UCRL-MA-106439, change 1, Feb 1996.